ACS Biomaterials SCIENCE & ENGINEERING

pubs.acs.org/journal/abseba

Article

Facile Detection of Blood Creatinine Using Binary Copper−Iron Oxide and rGO-Based Nanocomposite on 3D Printed Ag Electrode under POC Settings

Preeti Singh, Soumen Mandal,* Debolina Roy, and Nripen Chanda*

Cite This: https://doi.org/10.1021/acsbiomaterials.1c00484

Read Online

ACCESS | Metrics & More | Article Recommendations | Supporting Information

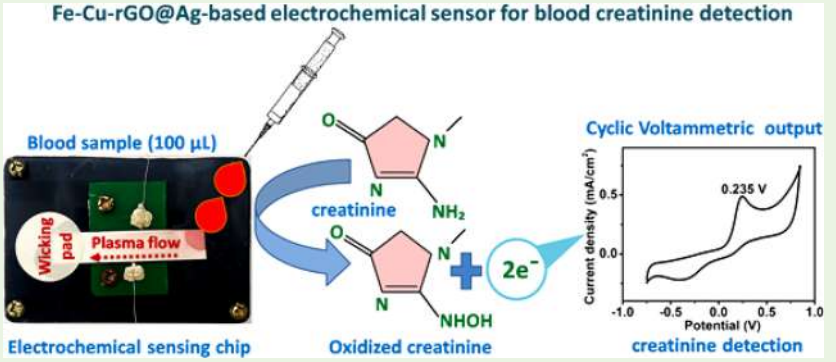

ABSTRACT: Metal nanoparticles have been helpful in creatinine sensing technology under point-of-care (POC) settings because of their excellent electrocatalyst properties. However, the behavior of monometallic nanoparticles as electrochemical creatinine sensors showed limitations concerning the current density in the mA/cm^2 range and wide detection window, which are essential parameters for the development of a sensor for POC applications. Herein, we report a new sensor, a reduced graphene oxide stabilized binary copper−iron oxide-based nanocomposite on a 3D printed Ag electrode (Fe−Cu−rGO@Ag) for detecting a wide range of blood creatinine (0.01 to 1000 μM; detection limit 10 nM) in an electrochemical chip with a current density ranging between 0.185 and 1.371 mA/cm^2 and sensitivity limit of 1.1 μA μM^{-1} cm^{-2} at physiological pH. Interference studies confirmed that the sensor exhibited no interference from analytes like uric acid, urea, dopamine, and glutathione. The sensor response was also evaluated to detect creatinine in human blood samples with high accuracy in less than a minute. The sensing mechanism suggested that the synergistic effects of Cu and iron oxide nanoparticles played an essential role in the efficient sensing where Fe atoms act as active sites for creatinine oxidation through the secondary amine nitrogen, and Cu nanoparticles acted as an excellent electron-transfer mediator through rGO. The rapid sensor fabrication procedure, mA/cm^2 peak current density, a wide range of detection limits, low contact resistance including high selectivity, excellent linear response (R^2 = 0.991), and reusability ensured the application of advanced electrochemical sensor toward the POC creatinine detection.

KEYWORDS: *binary, nanocomposite, 3D print, electrochemical sensing chip, creatinine detection, point of care*

INTRODUCTION

The creatinine level in blood serum is an essential indicator of various kidney and liver diseases. A deficient blood creatinine level signifies muscular dystrophy, poor liver functioning, and loss of body fluids. In contrast, high creatinine level indicates chronic kidney disease (CKD), which is a worldwide health crisis and can lead to chronic kidney failure when both the kidneys stop functioning.[1] Serum creatinine (SCr) levels for a normal healthy individual range between 40 and 150 μM (0.46−1.7 mg/dL),[2] whereas in extreme muscular dystrophy, the levels can fall as low as ∼10 μM (0.14 mg/dL).[3] The level shoots up to 442.1 μM (5 mg/dL) in the case of chronic kidney disease (CKD), leading to renal failure.[4−6] Thus, creatinine detection in human blood becomes an important measure of kidney and liver functioning and muscular dystrophy and can indicate the onset or presence of such diseases in human beings. Therefore, the development of an accurate method for routine quantitative creatinine measurement without any complicated sample preparation remains an important objective for detecting life-threatening diseases worldwide.

Received: April 9, 2021
Accepted: June 7, 2021

Several well-established methods, such as colorimetric, spectroscopic, and chromatographic techniques, have been widely used for creatinine detection.[7−11] However, tedious sample preparation, especially in colorimetric detection, and the requirement of sophisticated laboratory equipment, including lack of accurate quantitative measurement, restricts their applicability for rapid on-site monitoring and point of care diagnosis. On the other hand, electrochemical quantification using enzymatic biosensors represents a feasible laboratory-scale measurement technique.[12−14] However, the methods became complicated and less reliable because the immobilization of enzymes affects the biosensor shelf life in storage and operational stability.

Therefore, the development of simple and effective nonenzymatic techniques similar to the clinical diagnosis kits devices for the real-time monitoring of glucose is an important goal for point of care (POC) measurement of creatinine levels. A summary of prior work conducted for nonenzymatic electrochemical detection of creatinine and the gaps in these techniques are shown in Table S1.[12,15−28] As mentioned in Table S1, the existing literature reveals that although each exploration involves a unique creatinine detection method, significant gaps still exist. They are as follows: (i) the current responses of the sensors are low in the microamps range and (ii) the lowest and highest creatinine levels in human blood so far reported are out of detection limits. The low current range would lead to complex and bulk electronic circuitry, prohibitive in developing handheld devices to detect creatinine. Additionally, a POC device requires a wide range of detection, which should be greater than the range of creatinine levels reported in human blood. To address the issues mentioned above so that creatinine detection could be performed on handheld lab-on-chip devices, we report a new nonenzymatic creatinine detection sensor using rGO stabilized iron−copper binary nanoparticles electrodeposited over a 3D printed Ag electrode and an electrochemical chip. Furthermore, we report the interfacial mechanism for creatinine reaction with the said binary metal nanoparticles, causing higher response currents in the milliamp range for the first time.

As creatinine has several donor groups in its main tautomeric form, it can bind with various transition metal ions such as Ag(I), Hg(II), Cd(II), Zn(II), Co(II), Ni(II), Cu(II), Pt(II), and Pd(II) to generate redox currents. With this approach, various research groups have demonstrated creatinine detection using a monometallic platform.[24,27] However, in this work, the synergistic effect of Fe- and Cu-based binary nanoparticles is explored as their combination may possess better electrochemical performance than the monometallic nanoparticles.[29,30] The second approach of this work is to select a suitable support material for the distribution of binary nanoparticles for better stability and sustainable electrocatalytic activity. Reduced graphene oxide (rGO) meets these requirements as a support material because of its unique physicochemical properties with a high surface area, excellent electrical conductivity, good chemical as well as thermal stability, and low production cost. Combining rGO and binary nanoparticles could improve the nanocomposite electrocatalytic activity if used for an electrochemical reaction.[31−33] To achieve this synergistic effect, we conducted electrodeposition of the binary nanoparticles and rGO on a 3D printed electrode. Three-dimensional printing has several advantages over silk screen printed electrodes (SPE), as it allows design flexibility, rapid mask-free fabrication, ∼150 times lower resistivity (∼12 mΩ/cm^2 for 3D printed Ag electrodes) than Ag-SPEs (1.9 Ω/cm^2). All these benefits of the 3D printed electrode with the Fe−Cu−rGO nanocomposite made the overall electrochemical sensor, Fe−Cu−rGO@Ag, efficient for creatinine detection with respect to the higher response currents and better control over the resistivity by providing suitable electrode height, surface roughness, and higher porosity for promoting faster ionic diffusion followed by the catalytic electrochemical oxidation of creatinine.[34−37]

EXPERIMENTAL SECTION

Materials and Methods. Graphite flakes were purchased from Graphene Surpermarket, USA. Sodium acetate buffer solution (pH 5.2) and phosphate buffer solution (500 mL, 1 M, pH 7.4) were purchased from Sigma-Aldrich, USA. Analytical grade potassium hexacyanoferrate (III) ($K_3[Fe(CN)_6]$), potassium hexacyanoferrate (II) trihydrate ($K_4[Fe(CN)_6]\cdot 3H_2O$), sodium hydroxide, creatinine, urea, ferric chloride ($FeCl_3$), aniline, hydrochloric acid, sodium nitrite, and pH test strips were purchased from Merck (India) Pvt. Ltd. Analytical grade uric acid, glutathione, dopamine, copper(II) chloride dihydrate ($CuCl_2\cdot 2H_2O$), and iron(II) chloride tetrahydrate ($FeCl_2\cdot 4H_2O$) were procured from HiMedia Laboratories Pvt. Ltd., India. Isopropyl alcohol (propan-2-Ol) was purchased from Rankem, Avantor performance Materials, India. Whatman filter paper grade 1 and plasma separation membrane (PSM) were procured from Fisher Scientific, U.K.. and Cobetter Filtration Equipment Co. Ltd., China, respectively. Single-sided scotch tape was procured from Magic Tape, India and pipettes (5000, 1000, and 200 μL) were purchased from Tarson variable volume pipet, India. The printed circuit board (FR1 grade) and silver conductive ink was purchased from Voltera, UK. The silver conductive adhesive paste was purchased from Alfa Aesar, USA. The counter electrode (platinum wire of 0.5 × 35 mm, purity 99.99%, CHI115) and reference electrode (Ag/AgCl, CHI111) were purchased from CH Instruments, USA. Digital Multimeter, scissors, drilling machine, copper wire, and acrylic sheets, bolts and nuts were received from a local supplier. The experimental solutions and buffers were prepared with ultrapure Milli-Q water.

3D Printing of Silver Conductive to Prepare Interdigitated Pre-electrode. For the electrochemical detection of creatinine in blood plasma, the pre-electrodes were printed by 3D printing of conductive Ag ink on a flame retardant grade 1 (FR1) PCB substrate using a Voltera V-One conductive ink printer. The conductive ink comprises silver ink, 20% diethylene glycol monoethyl acetate, and 10% mineral spirits as specified by the manufacturer (Voltera datasheet; Conductor 2, SDS version 1.0). The PCB substrate was cut into a rectangular shape of 3.5 × 2.5 cm, and 3 printing of the conductive ink was performed in interdigitated fashion to develop a two-electrode system viz. working electrode (WE) and counter electrode (CE). First, the WE was printed two times with a fixed height of 400 μm. Copper wire was attached to the WE using silver conductive adhesive paste and kept at 50 °C for 2 h for proper drying and attachment. A continuity test was conducted to check the conductivity between the pre-electrodes and copper wire using digital multimeter. The 3D printed Ag electrode was next subjected to electrodeposition of Cu and Fe nanoparticles on rGO as nanocomposite to prepare the final electrochemical sensor, Fe−Cu−rGO@Ag.

Electrodeposition of Fe−Cu−rGO Nanocomposite on Ag Electrode to Prepare Fe−Cu−rGO@Ag Sensor. The Fe−Cu−rGO nanocomposite on a Ag electrode was synthesized in a stepwise manner. The graphite oxide was prepared from graphite flakes through well-known modified Hummer's method.[38] The obtained graphite flakes were then ultrasonicated for 3−4 h to get the well-dispersed graphene oxide (GO) in water (0.3 mg/mL, pH 3). The 10 mL GO solution (4.3 mg/mL) was prepared in 1× PBS (0.01 M) prior to electrodeposition on interdigitated Ag electrode. The cyclic voltammetry (CV) was carried out at a scan rate of 50 mV/s within the potential range from 0.5 to −1.5 V for 20 cycles. After

https://doi.org/10.1021/acsbiomaterials.1c00484
ACS Biomater. Sci. Eng. XXXX, XXX, XXX−XXX

Scheme 1. Fabrication of the Fe−Cu−rGO@Ag Sensor (WE) Interdigitated with Ag CE and Electrochemical Sensing Chip for Facile Detection of Blood Creatinine under POC Settings

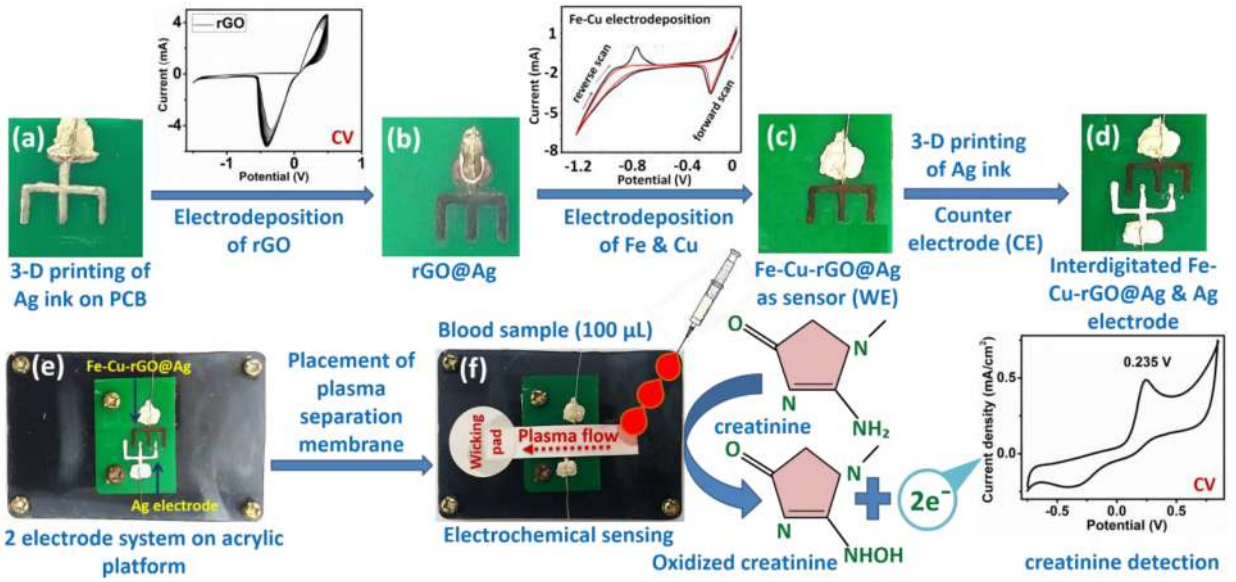

electrodeposition, the rGO electrode was gently washed with ultrapure water and dried at room temperature. Next, the direct electrodeposition method was followed to prepare the iron−copper−rGO nanocomposite on a Ag electrode. This step includes electrodeposition using mixed solution of $CuCl_2{\cdot}2H_2O$ and $FeCl_2{\cdot}4H_2O$ in sodium acetate buffer solution (pH 5.2) using a potential range from 0 to −1.2 V at a 50 mV/s scan rate. In this potential range, both the precursor of the iron and copper nanoparticles, i.e., Fe^{2+} and Cu^{2+} ions, were reduced on the rGO surface to form Fe−Cu−rGO. After the successful preparation of Fe−Cu−rGO@Ag (WE), a CE was printed following the same aligned 3D printing technique as described above to generate an interdigitated electrode pattern. For comparison study, only rGO, Cu−rGO, and Fe−rGO were deposited on the Ag electrode following the above-described procedure. The copper wire was attached to the interdigitated CE and WE using silver conductive adhesive paste and kept at 50 °C for 2 h for proper drying and attachment.

The characterization of the Fe−Cu−rGO nanocomposite on the Ag electrode was either performed directly or after careful removal of the material from the electrode. The surface morphology, shape, dispersity, and elemental mapping were analyzed by a field-emission scanning electron microscope (FESEM) (Zeiss Sigma HD), operated at an electron high tension (EHT) of 5.0 kV. The iron and copper electronic states and chemical composition were determined using X-ray photoelectron spectroscopy (XPS, PHI 5000 Versa Probe II, FEI Inc.). The crystalline nature of the Fe−Cu−rGO was determined through a powder X-ray diffractometer (PANalytical Empyrean XRD), at 2θ Bragg's angle range between 15 and 80°. The structural disorder and defects in the graphitic matrix were studied by Raman spectroscopy (WITEC 300 RAS instrument). Electrochemical properties of the Fe−Cu−rGO on a Ag electrode were investigated in an electrochemical sensing chip-based system using cyclic voltammetry (CV), differential pulse voltammetry (DPV), and electrochemical impedance spectroscopy (EIS) (Bio Logic Science Instrument, SP-150).

Electrochemical Characterization of Fe−Cu−rGO@Ag. An electrochemical sensing chip was developed to accommodate Fe−Cu−rGO@Ag as WE and Ag as CE to study the electrochemical properties of the sensor using cyclic voltammetry (CV) and electrochemical impedance spectroscopy (EIS) and with respect to a 5.0 mM concentration of the ferro/ferricyanide solution mixture ($Fe(CN)_6^{4-}$:$Fe(CN)_6^{3-}$ = 1:1 molar ratio; 2.5 mM each in 0.01 M PBS as standard redox solution). The chip with dimensions 7.2 cm length and 4.6 cm width consisted of a rectangular PCB (3.5 cm length × 2.5 cm width) with a 3D printed Ag electrode (CE) and a Fe−Cu−rGO@Ag sensor (WE) that was individually connected by copper wires using silver adhesive. A plasma separation membrane (PSM) of dimensions 4.0 cm length and 0.7 width covering both electrodes was placed on the PCB in such a way that creatinine solution or blood plasma can flow over the electrodes for the electrochemical reaction on application of potential voltage. A wicking pad (circular, 2.0 cm in diameter), made of Whatman filter paper, was place at the end of the membrane to assist the flow of the solution and absorb excess solution after the electrochemical reaction on the chip. To perform the electrochemical studies, a potential range of −1.0 V to +1.0 V and back to −1.0 V was applied at 50 mV/s scan rate. The analysis was performed based on the shift of peak current density or change in charge-transfer resistance due to the change in the surface charge at the working electrode surface when oxidation of $Fe(CN)_6^{4-}$ to $Fe(CN)_6^{3-}$ and the reduction of $Fe(CN)_6^{3-}$ to $Fe(CN)_6^{4-}$ occurred in PBS (0.01 M) buffer. The impedance related information on the Fe−Cu−rGO@Ag was obtained by fitting the data with a Randles equivalent circuit using *ZSimpWin* V 3.21 software.

Sensitivity Analysis of Creatinine Using Fe−Cu−rGO@Ag. The detection ability of the sensor, i.e., Fe−Cu−rGO@Ag, was performed with different concentrations of creatinine in 0.01 M PBS through cyclic voltammetry (a scan rate of 50 mV/s within the potential range from −0.8 V to +0.8 V back to −0.8 V), differential pulse voltammetry, and electrochemical impedance spectroscopy. The plasma separation membrane was used to flow the various concentrations of the creatinine, i.e., 0 (blank), 0.01, 0.1,1, 5, 10, 100, 200, 300, 400, 500, 600, 750, and 1000 μM into the electrochemical sensing chip for sensitivity analysis.

Repeatability, Reproducibility, Stability, and Reusability of Fe−Cu−rGO@Ag. The repeatability study of Fe−Cu−rGO@Ag was determined with 100 μM creatinine solution in 0.01 M PBS using CV technique. The CV was recorded repeatedly with the Fe−Cu−rGO@Ag electrode for 10 cycles at a 50 mV/s scan rate. The oxidation peak current density obtained from each cycle was plotted and relative standard deviation (RSD) was calculated to determine the repeatability of the sensor. For the reproducibility study of Fe−Cu−rGO@Ag, four individual sensors were newly prepared by electrodeposition and investigated using 100 μM creatinine solutions via CV techniques. Each sensor was scanned for 10 consecutive cycles at a scan rate of 50 mV/s. The oxidation peak current density obtained from individual sensor was plotted and relative standard deviation (RSD) was calculated to determine the reproducibility of

https://doi.org/10.1021/acsbiomaterials.1c00484
ACS Biomater. Sci. Eng. XXXX, XXX, XXX−XXX

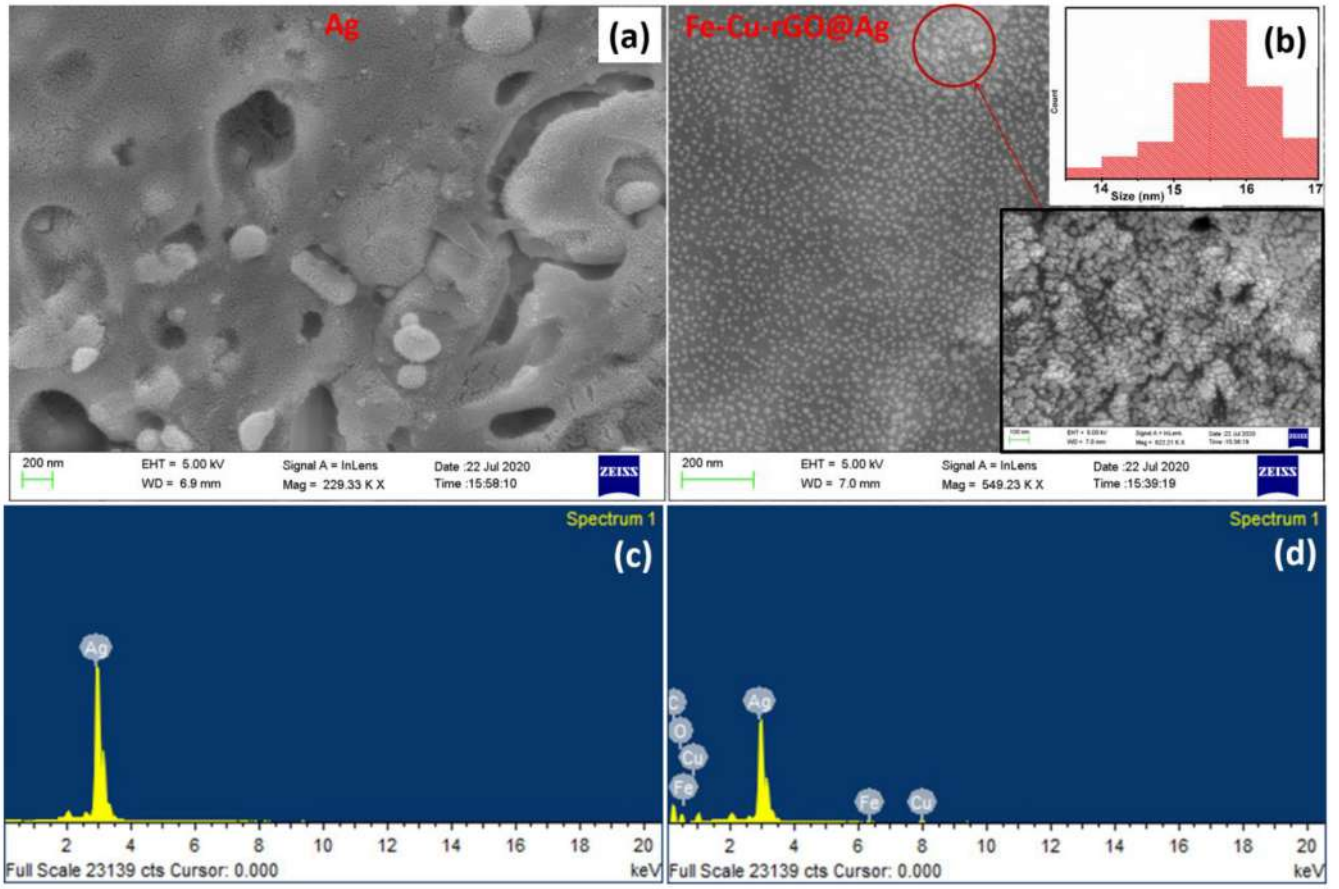

Figure 1. Comparative FESEM images of (a) Ag and (b) Fe−Cu−rGO@Ag; (c) energy-dispersive X-ray spectroscopy (EDS) of Ag and (d) Fe−Cu−rGO@Ag; Inset in b: Overall Cu/Fe nanoparticle size distribution (15−16 nm range) on rGO surface.

the sensor. The sensor stability was measured periodically for 10 weeks. Each time, the CV was performed 10 times and monitored the electrochemical stability with respect to the change in oxidation peak current density. The CV graph obtained from the sensor at each week was plotted to determine the stability of the sensor. To check the reusability of the sensor after every week, we carefully washed the sensor with 0.01 M PBS before and after the CV scans.

Interference Study. Interfering molecules such as uric acid, urea, dopamine and glutathione were tested at their detectable concentrations (uric acid, 100.0 μM; urea, 1.0 mM; dopamine, 100.0 μM; and glutathione, 50.0 μM) in PBS solution (0.01 M) in the presence of 0.1 mM (100 μM) creatinine. Cyclic voltammetry and differential pulse voltammetry graphs were recorded for these experiments. The sensor electrode was found to be sensitive and selective even in the presence of the commonly interfering species.

Analysis with Whole Blood Sample. The whole blood samples were collected from Durgapur Steel Plant (DSP) Hospital, West Bengal, India, with the consent of healthy volunteers. For the analysis, the whole blood was used as received without any further purification. The plasma separation membrane was used to separate out the plasma from whole blood and allowed to flow to the detection zone. One hundred microliters of whole blood were carefully poured over the plasma separation membrane that was placed over the electrodes to make them moist with the plasma fluid and cyclic voltammetry (50 mV/s scan rate) and differential pulse voltammetry data were recorded. Spiking with different concentrations of creatinine was also performed for the detection using standard addition techniques.

The Fe−Cu−rGO@Ag sensor reusability was studied by cleaning the counter and working electrode with 0.01 M PBS (pH 7.4). CV was carried out for 50 cycles at a scan rate of 50 mV/s within the potential range from −1.0 V to +1.0 V back to −1.0 V that successfully cleanses and refreshes the sensor for another use.

It is of note that all the studies with human blood samples were performed with approval from the institutional ethical committee (IEC) of CSIR-Central Mechanical Engineering Research Institute, Durgapur. As suggested by the members, the blood sample wastes were disposed of in a strong bag after autoclaving.

RESULTS AND DISCUSSION

Characterizations of Fe−Cu−rGO@Ag. Scheme 1 s1 represents the image of an electrochemical sensing chip for the detection of plasma creatinine in whole blood under POC settings. In the chip, one of the 3D printed silver (Ag) electrodes with iron−copper−rGO nanocomposite was used as electrochemical sensor (Fe−Cu−rGO@Ag, WE), whereas the other one was used as the CE in an interdigitated configuration. The Fe−Cu−rGO−based nanocomposite was prepared in two steps. The first step includes the electrodeposition of graphene oxide (GO) as its reduced form, i.e., reduced graphene oxide (rGO) on the bare 3D printed Ag electrode (rGO@Ag) by applying a potential range of 0.5 to −1.5 V (Figure S1a).[39] Next, iron (Fe) and copper (Cu) were codeposited in nanoparticulate form on rGO@Ag electrode by electrochemical redox reaction with the Fe^{2+} and Cu^{2+} ions using a potential range of 0 to −1.2 V versus Ag/AgCl. During coelectrodeposition, the anodic and cathodic scans displayed two prominent reduction and oxidation peaks. The peak at −0.20 V attributed to the reduction of Cu^{2+} to Cu^0 while the peak located at −0.73 V was due to the oxidation of Fe^{2+} to Fe^{3+} as shown in Figure S1b.[40,41] It is worth mentioning that the deposition of Cu^0 happened in the first cycle of CV itself as

https://doi.org/10.1021/acsbiomaterials.1c00484
ACS Biomater. Sci. Eng. XXXX, XXX, XXX−XXX

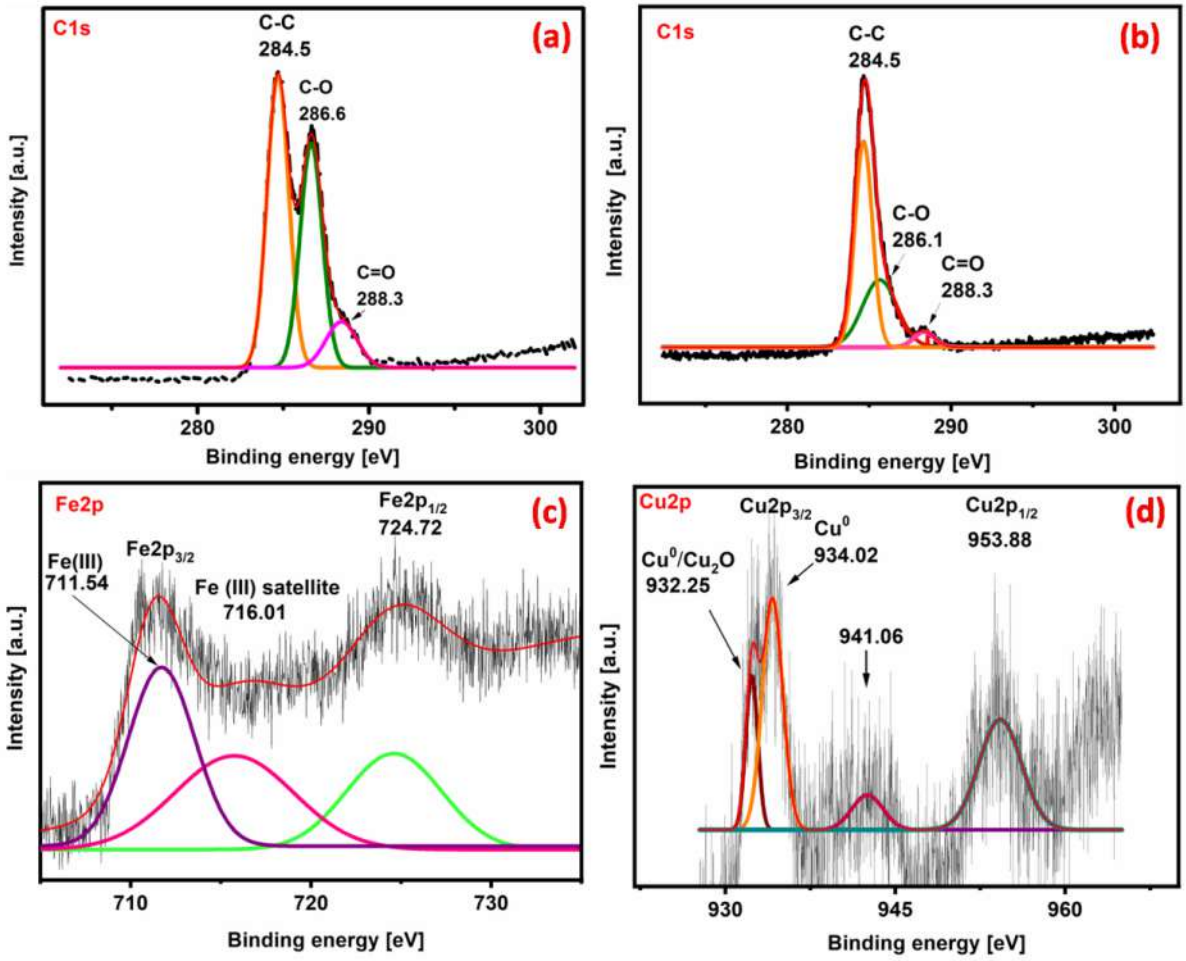

Figure 2. Chemical composition analysis of GO and Fe−Cu−rGO@Ag using deconvoluted XPS for; (a) C 1s spectrum of GO, (b) C 1s spectrum of Fe−Cu−rGO@Ag, (c) Fe 2p spectrum of Fe−Cu−rGO@Ag, and (d) Cu 2p spectrum of Fe−Cu−rGO@Ag.

shown by a sharp peak at −0.20 V and there was no reduction peak for Fe^{2+} to Fe^0 deposition. However, as the electrochemical cycles continued, the delayed deposition of Fe^{3+} occurred at −0.73 V during the reverse scan, suggesting the fact that the deposition of copper (Cu^0) and iron (in the form of Fe^{III}-oxide) sequentially happened on the rGO@Ag.

The obtained Fe−Cu−rGO-based nanocomposite on the Ag electrode was characterized either directly on the electrode or after careful removal from the electrode using FESEM, EDS, XPS, XRD, and Raman. Figure 1 shows the surface characterization using the FESEM technique for the Ag and Fe−Cu−rGO@Ag sensor electrode surfaces. The characteristic flakelike structures are observed on the bare Ag electrode surface (Figure 1a), whereas electrodeposition of iron and copper results in granular-shaped nanoparticles (Figure 1b).

Figure 1b also shows the difference in contrast among the nanoparticles. The uneven distribution of cauliflower-like structures might be due to the formation of Fe nanoparticles on the homogeneously distributed spherical Cu nanoparticles that were formed first during the cathodic scan of the electrodeposition and stabilized by the rGO present on Ag-electrode.[42] The size distribution of the Fe−Cu nanoparticles shown in the inset to panel b was measured using *ImageJ* indicates a size range of 15−16 nm. From the energy-dispersive X-ray absorption spectroscopy (EDS) spectrum, it clearly indicates the presence of Ag element on the bare surface, while after the successful electrodeposition of the iron and copper, the electrode surface shows considerable amount of Fe, Cu, O, and C with Fe/Cu ratio of 1:3 wt % (Figure 1c, d).

X-ray photoelectron spectroscopy (XPS) measurements were performed to analyze the chemical states of iron and copper after electrodeposition. The C 1s spectrum of only GO shows three peaks at 284.5, 286.6, and 288.3 eV after deconvolution, which corresponds to the C−C, C−OH, and sp^2-hybridized carbon atoms of C═O bonds, respectively (Figure 2a). After the electrodeposition of rGO followed by Fe and Cu, the intensities for the C−OH and C═O bonds decrease significantly, which justifies the loss of the −COOH, −O−, and −OH groups due to reduction of GO to rGO (Figure 2b).[43] In the deconvoluted Fe 2p XPS spectrum shown in Figure 2c, two asymmetric peaks at binding energies of 711.54 eV (Fe $2p_{3/2}$) and 724.72 eV (Fe $2p_{1/2}$) with a satellite peak at 716.01 are signature peaks for the Fe^{3+} form of iron oxide. These peaks certify that the iron oxide in nanocomposite is in Fe_2O_3 form (Figure 2c). Copper deconvolution in Figure 2d shows two major peaks of Cu 2p at 932.25 and 953.88 eV corresponding to the Cu^{1+} of Cu_2O.[44] Also, a strong peak is observed at 934.02 eV that is assigned to Cu^0 state.[45] The satellite peak at approximately 941.06 eV may be due to metallic copper and/or partially oxidized copper.[46]

The XRD spectrum of the iron−copper-based nanocomposite illustrates five characteristic diffraction peaks at 2θ

https://doi.org/10.1021/acsbiomaterials.1c00484
ACS Biomater. Sci. Eng. XXXX, XXX, XXX−XXX

of 26.93° (112), 32.81° (122), 39.24° (123), 53.85°(115), and 63.4°(205), which confirms the crystalline structure of the present iron oxide is in the form of Fe_2O_3 as shown in Figure 3

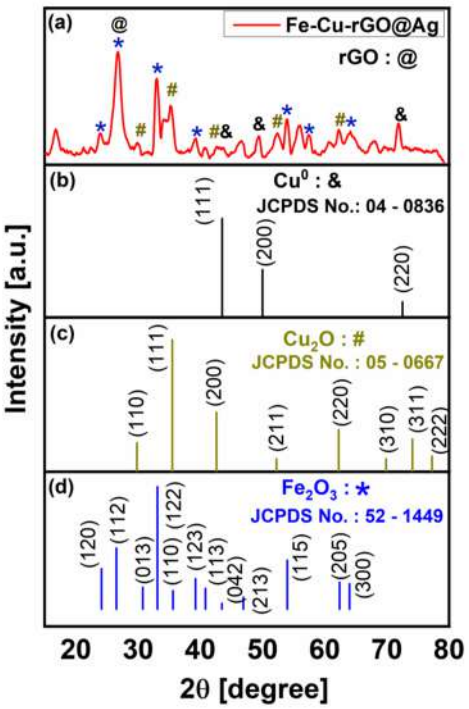

Figure 3. (a) XRD pattern of Fe−Cu−rGO nanocomposite; comparative XRD patterns of (b) Cu0 (JCPDS No. 04−0836), (c) Cu2O (JCPDS No. 05−0667), and (d) Fe2O3 (JCPDS No. 52−1449).

(JCPDS No. 52−1449). The XRD peaks at 2θ values of 43.4° (111), 50.4° (200), and 72.51° (220) indicate the presence of metallic copper (Cu^0) in the nanocomposite (JCPDS No. 04−0836).[40] The XRD patterns with five diffraction peaks at 29.6° (110), 35.6° (111), 42.1° (200), 52.33° (211), and 62.1° (220) confirm the presence of cuprous oxide (Cu_2O) structure (JCPDS No. 05−0667).[44,45] The presence of cuprous oxide in the nanocomposite may be due to the oxidative-addition reaction of surface Cu-atoms of the bulk Cu^0 nanoparticles with rGO during stabilization. The characteristic peak of reduced graphene oxide at 2θ of 26.93° (002) designates the reduction of oxygen functional groups of graphene oxide in the electrodeposited Fe−Cu−rGO nanocomposite on the Ag electrode.[47]

The in situ change of GO to rGO is confirmed by Raman spectroscopy studies, which is widely used to characterize the structural disorder, and defects in chemically synthesized graphene-based materials. It is reported that the I_D/I_G ratio increases from graphite to graphene oxide (GO) and again decreases after conversion of GO to rGO.[48] Figure S2 demonstrates the intensity of the D band at ∼1356 cm^{-1} corresponding to the disorder in the sp^2 carbon network decreases in Fe−Cu−rGO. On the other hand, the G band at ∼1575 cm^{-1} for the tangential vibrations of the sp^2 carbon atoms in the hexagonal planes increases in comparison to the GO. The I_D/I_G ratio of Fe−Cu−rGO becomes ∼0.86, which specifies the conversion of GO to rGO by eliminating most of the oxygen-containing functional groups and consequently increasing the usual size of the sp^2 domains.[49]

The existence of Cu^0- and Fe^{3+}-based nanoparticles in the nanocomposite was further investigated by cyclic voltammetry (CV) in 0.1 M NaOH (Figure S3). The anodic and cathodic scans display three oxidation and reduction peaks. The oxidation peaks at potentials of −0.236 V (a) and 0.235 V (b) are attributed to the oxidation of Cu^0 to Cu^{1+} and Cu^{1+} to Cu^{2+}, respectively. The reduction peaks at potentials of −0.031 V (b′) and −0.715 V (a′) represent the transition of Cu^{2+} to Cu^{1+} and of Cu^{1+} to Cu^0, respectively. The redox peak located at 0.576 V (c) and 0.245 V (c′) may be due to the oxidation and reduction of Fe^{2+} to Fe^{3+} and vice versa (Figure S3).[50] The appearance of the CV peaks, i.e., c and c′ was expected as it is reported that the adsorption of Fe^{II}−OH can happen on positively charged Fe_2O_3, without changing the surface properties of Fe_2O_3, which ultimately oxidizes to Fe^{3+} and is built into the bulk structure of Fe_2O_3.[51] The electrochemical behavior of these nanocomposite-modified electrodes well agreed with XPS, XRD, and Raman results. On the basis of these results, it is confirmed that Fe−Cu−rGO nanocomposite on the Ag surface consists of metallic copper nanoparticles and Fe_2O_3 nanoparticles, which are adhered to the rGO surface and provide multiple adsorption sites for direct interaction with creatinine during its detection.

Study of Fe−Cu−rGO@Ag in an Electrochemical Sensing Chip. The suitability of Fe−Cu−rGO@Ag as a

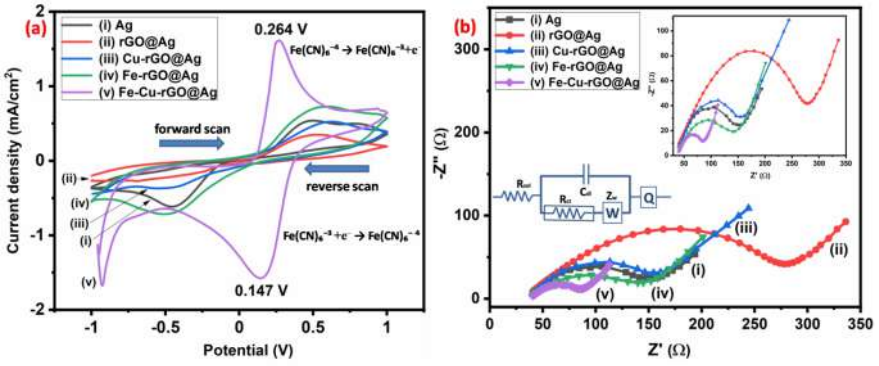

Figure 4. (a) CV graphs of 5.0 mM concentration of ferro/ferricyanide solution (1:1 ratio) in PBS using (i) Ag, (ii) rGO@Ag, (iii) Cu−rGO@Ag, (iv) Fe−rGO@Ag, and (v) Fe−CurGO@ Ag (sensor) electrodes at scan rate of 50 mV/s; (b) EIS recorded with frequency range from 10 kHz to 1 Hz using (i) Ag, (ii) rGO@Ag, (iii) Cu−rGO@Ag, (iv) Fe−rGO@Ag, and (v) Fe−Cu−rGO@Ag electrodes to demonstrate the electrocatalytic activity of the sensor.

https://doi.org/10.1021/acsbiomaterials.1c00484
ACS Biomater. Sci. Eng. XXXX, XXX, XXX−XXX

sensor was evaluated in the electrochemical sensing chip (Scheme 1). The detailed dimensions of the chip with the two interdigitated electrode configurations are shown in Figure S4. To compare the electrochemical behavior of the Fe−Cu−rGO@Ag; Ag, rGO@Ag, Cu−rGO@Ag, and Fe−rGO@Ag electrodes were also tested using CV and EIS techniques and 5.0 mM ferro/ferricyanide solution ($Fe(CN)_6^{4-}$:$Fe(CN)_6^{3-}$ = 1:1 molar ratio; 2.5 mM each) at a scan rate of 50 mV/s within the potential range from −1.0 V to +1.0 V back to −1.0 V (Figure 4a).

The bare Ag electrode shows anodic and cathodic peak potentials at 0.471 V and −0.496 V attributed to $Fe^{2+/3+}$ redox couple at pH 7.4. However, when rGO was deposited, the rGO@Ag electrode performance becomes inferior (Figure 4a). The reason for such behavior may be due to the less conductive property of rGO (with incomplete graphene structure) that can minimally take part in the interfacial electron transfer process, resulting in a low current response from the ferro/ferricyanide redox couple.[52] On the other hand, the current density for the Fe−Cu−rGO@Ag increased in both oxidation and reduction scan at 0.264 and 0.147 V, respectively, with a decrease in ΔE (117 mV) as compared to the Ag, rGO@Ag electrodes (967 mV and 991 mV). The lowest ΔE might be due to the presence of Fe_2O_3 and Cu nanoparticles on the rGO network within the nanocomposite where Fe_2O_3 provide the platform for the redox reaction of $Fe(CN)_6^{4-}$/$Fe(CN)_6^{3-}$, whereas the adjacent Cu nanoparticles work as an excellent electron mediator for the charge transfer between ferro/ferricyanide solution and the electrode surface. Besides, the presence of binary nanoparticles increases the active surface area of the Fe−Cu−rGO@Ag sensor for the direct electron transfer and the combination of all these activities help to exhibit high electrocatalytic behavior toward the redox reaction $Fe(CN)_6^{4-}$ to $Fe(CN)_6^{3-}$ and vice versa.[53] The diffusion coefficient (D) of $Fe(CN)_6^{4-}$/$Fe(CN)_6^{3-}$ for Fe−Cu−rGO@Ag was calculated following the Randles−Sevcik equation considering irreversible redox reaction as sensor electrode:[54,55]

$$I_p = 2.99 \times 10^5 n^{3/2} \alpha^{1/2} A C D^{1/2} v^{1/2} \quad (1)$$

where I_p (peak current of the electrode, anodic/cathodic) = 0.00061 Amp, n (number of electrons for $Fe(CN)_6^{4-}$/$Fe(CN)_6^{3-}$) = 1, A (surface area of electrode) = 0.38 cm^2, D (diffusion coefficient), C (concentration of $Fe(CN)_6^{3-/4-}$) = 5 × 10^{-6} mol/cm^3, and v (scan rate) = 0.05 V/s. The electron transfers coefficient (α) was calculated following the reported procedure by Wang et al. (see the Supporting Information).[55] By incorporating appropriate values in eq 1 above, the D value was obtained as 3.43 × 10^{-5} cm^2 s^{-1} for Fe−Cu−rGO@Ag which is higher than the recently reported one.[26] The high value of D for Fe−Cu−rGO@Ag may be due to the high aspect ratio of electrode surface and associated electrostatic interactions between the electrode surface and the redox species that provides a facile transportation of $Fe(CN)_6^{3-/4-}$ from bulk to the electrode. Further, the impedance measurement was performed in a frequency range of 10.0 kHz to 1.0 Hz to understand the electrocatalytic behavior of the sensor electrode (Figure 4b). The decreased radius of the semicircle at high frequency indicates that the charge-transfer resistance (R_{ct}) is significantly decreased, consistent with the CV curves (Figure 4a). The R_{ct} relates to the electron-transfer kinetics of the analytes along with its diffusion control process in the case of irreversible redox reaction at the electrode interface. As expected, Fe−Cu−rGO@Ag showed a significantly lower internal charge-transfer resistance than the other electrodes of the present study, indicating a conductive pathway of electrons toward the electrode for signal generation. Figure 4b (inset) shows the Randles circuit model to determine the charge transfer resistance (R_{ct}) value of all the electrodes including the Fe−Cu−rGO@Ag sensor, tabulated in Table S2. Further, the R_{ct} value was used to determine the heterogeneous charge transfer rate constant (K^0) of $Fe(CN)_6^{4-}$/$Fe(CN)_6^{3-}$ for Fe−Cu−rGO@Ag. The K^0 was calculated using the following equation:[56]

$$K^0 = RT/n^2F^2AR_{ct}C \quad (2)$$

where R (gas constant) = 8.314 J mol^{-1} K^{-1}, T (temperature) = 298 K, F (Faraday constant) = 96 500 C mol^{-1}, R_{ct} (charge transfer resistance) = 82.66 Ω, whereas n, A, and C values were similar as above. By incorporating the values in eq 2, the K^0 value was obtained as 1.694 × 10^{-3} cm s^{-1} for Fe−Cu−rGO@Ag, which is better as compared to the reported values.[56] Moreover, the surface concentration (C) of the adsorbed $Fe(CN)_6^{4-}$/$Fe(CN)_6^{3-}$ on the sensor was calculated following the Brown−Anson model equation:[57]

$$I_{pa} = (n^2F^2CAv)/4RT \quad (3)$$

where I_{pa} (oxidation peak current for $Fe(CN)_6^{4-}$/$Fe(CN)_6^{3-}$) = 0.00061 A, C (surface concentration of $Fe(CN)_6^{3-/4-}$), whereas A, v, R, and T were used as given above. After using these vales in eq 3, the surface concentration of $Fe(CN)_6^{3-/4-}$ was obtained as 3.46 × 10^{-8} mol cm^{-2}, which is due to the high surface area of Fe−Cu−rGO@Ag that permits a significant degree of coverage to $Fe(CN)_6^{4-}$/$Fe(CN)_6^{3-}$ species. The lowest R_{ct}, and high K^0 value of the Fe−Cu−rGO@Ag might be due to the synergistic effect of the network structure of rGO and Cu−Fe_2O_3 nanoparticles. In addition to that, the absorbed surface concentration of $Fe(CN)_6^{4-}$/$Fe(CN)_6^{3-}$ on the sensor enhanced the current density to a measurable output (in mA/cm^2 range). All these factors collectively decreased the overpotential toward better electrocatalytic property, which became useful to use as an electrochemical sensor for creatinine detection.

Electrochemical Detection of Creatinine: Study of Sensitivity, Selectivity, and Associated Mechanism. The sensing performance of the Fe−Cu−rGO@Ag in the electrochemical chip was estimated using 100.0 μM of creatinine solution within the potential range from −0.8 V to +1.4 V back to −0.8 V. The sensor performance was also compared with bare Ag, rGO@Ag, Cu−rGO@Ag, and Fe−rGO@Ag electrodes under identical condition. As shown in Figure S5a, no redox peak potential appeared in the absence of creatinine in PBS with Fe−Cu−rGO@Ag; however, after the addition of 100 μM of creatinine, a current response is observed at 0.235 V due to the oxidation of the added analyte. In Fe−rGO@Ag electrode, a current response is observed at 0.251 V, whereas the bare Ag, rGO@Ag, and Cu−rGO@Ag do not show any significant response for creatinine (Figure S5b, inset). The anodic peak current density (I_a) and anodic peak potential (E_a) for Fe−rGO@Ag and Fe−Cu−rGO@Ag are 0.072 mA/cm^2, 0.251 V and 0.352 mA/cm^2, 0.235 V, respectively. The higher I_a and lower E_a indicate that Fe−Cu−rGO@Ag has the electrocatalytic property that contributes to creatinine oxidation and is better than the other electrodes at detecting

https://doi.org/10.1021/acsbiomaterials.1c00484
ACS Biomater. Sci. Eng. XXXX, XXX, XXX−XXX

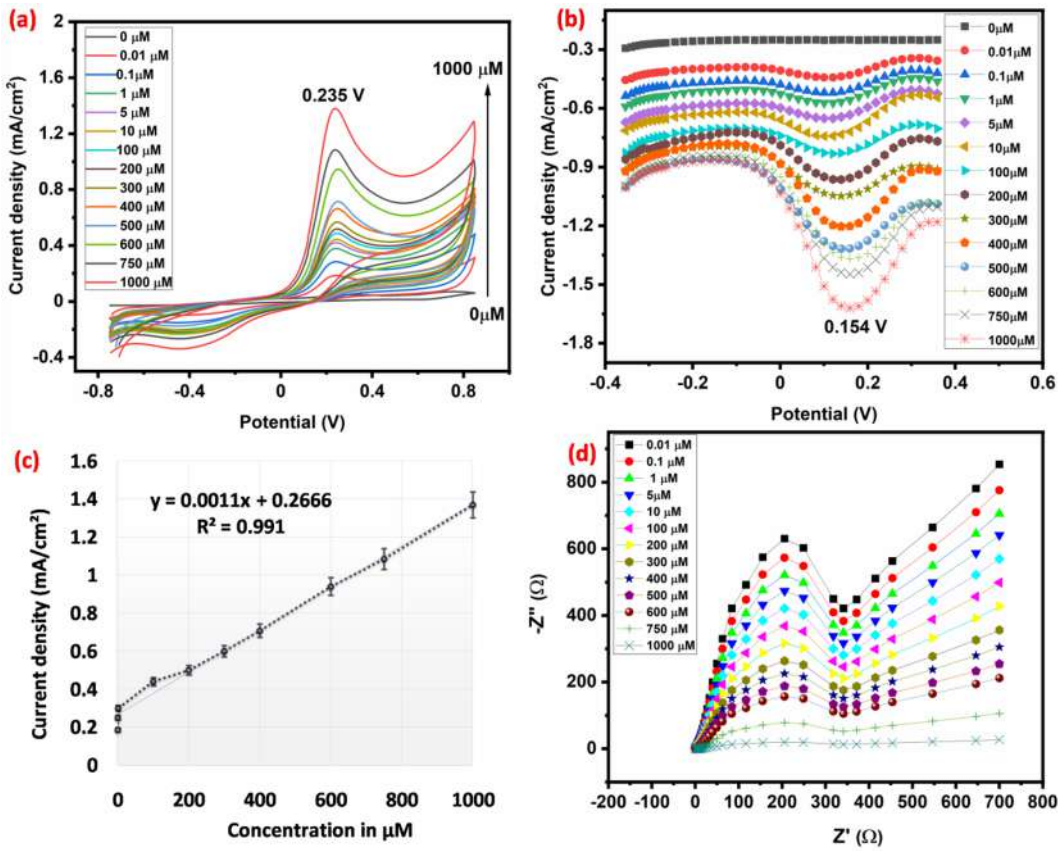

Figure 5. (a) CV and (b) DPV of different concentrations of creatinine (blank, 0.01, 0.1, 1, 5, 10, 100, 200, 300, 400, 500, 600, 750, and 1000 μM) using Fe−Cu−rGO@Ag electrode (area = 0.38 cm^2) in 0.01 M PBS (pH 7.4) at a scan rate of 50 mV/s; (c) linear regression curve of creatinine concentrations versus current density with an R^2 value of 0.991 and a sensitivity of 1.1 μA μM^{-1} cm^{-2}; (d) EIS of all concentrations of creatinine (frequency range of 10.0 kHz to 1.0 Hz).

creatinine in buffer medium (pH ∼7.4). To demonstrate the sensitivity of Fe−Cu−rGO@Ag, we performed CV and DPV studies with various concentrations of creatinine (0.01, 0.1, 1, 5, 10, 100, 200, 300, 400, 500, 600, 750, and 1000 μM) in 0.01 M PBS (∼pH 7.4) within the potential range from −0.8 V to +0.8 V back to −0.8 V (Figure 5a, b). Both CV and DPV show an increase in the current densities from 0.185 to 1.371 mA/cm^2 at 0.235 V and from 0.435 to 1.63 mA/cm^2 at 0.154 V, respectively, due to increasing creatinine concentration from 0.01 to 1000 μM. The increase in current density is linear with a limit of detection of 0.01 μM (10 nM) (R^2 = 0.991), as shown in Figure 5c. The calculated sensitivity from the linear calibration curve slope is 1.1 μA μM^{-1} cm^{-2}, as, which is comparable to or better than the reported electrochemical-based creatinine sensors, as summarized in Table S1.

Like the $Fe(CN)_6^{4-}/Fe(CN)_6^{3-}$ redox reaction, the creatinine oxidation is an irreversible process and involves both diffusion as well as adsorption of creatinine for charge transfer at the sensor electrode surface. For this reason, the diffusion coefficient (D), the surface concentration of creatinine (C) after diffusion, and the heterogeneous charge transfer rate constant (K^0) for creatinine oxidation at the sensor surface were calculated to be 1.84×10^{-3} cm^2 s^{-1}, 2.33×10^{-9} mol cm^{-2}, and 5.08×10^{-3} cm s^{-1} (see Tables S3 and S4 and the associated equations). The calculated values of diffusion coefficient (D) and concentration of creatinine (C), and charge transfer rate constant (K^0) found to be better as compared to other reported values for electrochemical creatinine detection.[25,26] These values support the statement that Fe−Cu−rGO-based nanocomposite plays a significant role in the electrochemical sensing of creatinine as upon increasing creatinine addition, more and more creatinine binds with the nanocomposite active sites, leading to an increase in the current density manifold as demonstrated in CV and DPV studies.

Interestingly, the adsorption of creatinine molecules at the electrode interface does not affect the internal resistance and reactance of the overall electrochemical system, as the impedance value decreases without changing the electron-transfer resistance (R_{ct}), whereas the creatinine concentration increases within the frequency range from 10 kHz to 1 Hz (Figure 5d). The constant value of the electron-transfer resistance (R_{ct}) also suggests that assembly of creatinine occurs at one interface, i.e., on the surface of the Fe_2O_3 nanoparticles of the Fe−Cu−rGO@Ag electrode, whereas Cu nanoparticles play an important role in carrying electrons from the analyte to the electrode for detectable signal processing.

Next, it became essential to explore the mechanism of Fe−Cu−rGO@Ag electrocatalytic oxidation of creatinine during its detection (Scheme 2 and Figure 6). Pure rGO usually exhibits low electrical conductivity due to few sp^3 carbons in the rGO matrix. After the deposition of highly conductive Cu nanoparticles on the rGO surface, the Cu−rGO@Ag shows a limited performance because of the lack of interfacial creatinine binding sites for its oxidation. Interestingly, it has been reported that Fe_2O_3 can serve as active interfacial sites for

https://doi.org/10.1021/acsbiomaterials.1c00484
ACS Biomater. Sci. Eng. XXXX, XXX, XXX−XXX

Scheme 2. Mechanism of Creatinine Oxidation on the Fe−Cu−rGO@Ag Electrode

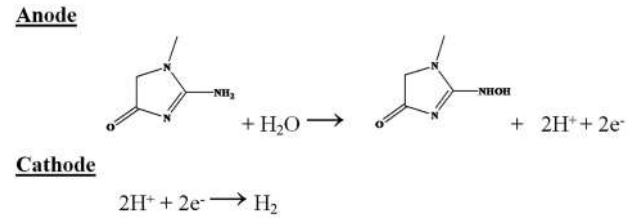

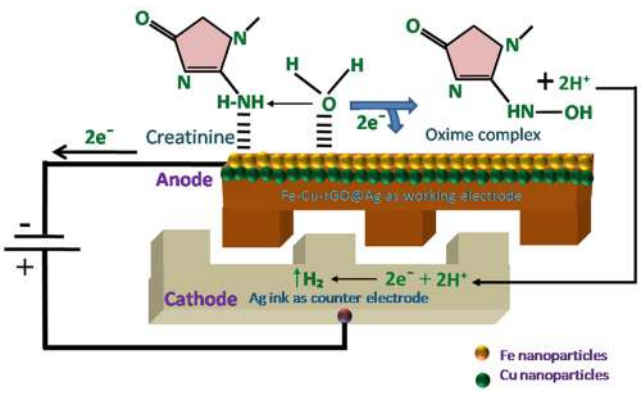

Figure 6. Mechanism of electrocatalytic oxidation of creatinine by Fe−Cu−rGO@Ag electrode.

creatinine oxidation because unsaturated surface Fe atoms of Fe_2O_3 can efficiently capture creatinine through the secondary amine nitrogen and Fe^{3+} interaction. Thus, the presence of Fe_2O_3 in Fe−rGO@Ag slightly improved creatinine oxidation because of the rapid immobilization of creatinine molecules on the Fe−rGO@Ag surface for the electron transfer through rGO. However, when CuNP is loaded, followed by Fe_2O_3 on the rGO surface, significantly enhanced the electrocatalytic oxidation of creatinine to its oxime occurs in the presence of water molecules. The formation of oxime is confirmed by the spot test for the oxime. This test developed a bluish-green color solution in the presence of diazonium salt and ferric chloride in alkaline pH on the plasma separation membrane used in the chip during the creatinine sensing process (Figure S6).[58]

The improved performance can be attributed to the excellent synergistic effect of CuNP as an electron-transfer mediator and Fe_2O_3 as active interfacial sites for creatinine molecules. It assumes that, after incorporating the highly conductive Cu nanoparticles between the rGO@Ag and the Fe_2O_3, the electrochemically generated electrons during the oxidation of creatinine on Fe_2O_3 rapidly transfer to the current collector, i.e., Ag through the CuNP for signal generation. Of note, the modified electrodes, Cu−rGO@Ag and F−rGO@Ag, show peaks at 0.63 and 0.59 V, respectively, whereas the Fe−Cu−rGO@Ag shows a peak at 0.264 V for ferro/ferricyanide reaction (Figure 4a), confirming the electrocatalytic activity of Fe_2O_3 over CuNP by reducing the overpotential of individual CuNP and Fe_2O_3@Ag. Therefore, a combination of Fe_2O_3-based interfacial active sites for creatinine binding and CuNP-mediated fast electron-transfer pathway play an important for the present electrochemical sensing of creatinine. The schematic representation of the mechanism is shown below:

Repeatability, Reproducibility, Stability, and Reusability of Fe−Cu−rGO@Ag Electrochemical Sensing Chip. Repeatability, reproducibility, stability, and reusability of a sensor are the most important factors to develop a chip-based device for point-of-care use. The repeatability study of Fe−Cu−rGO@Ag was determined with 100 μM creatinine solution in 0.01 M PBS using the CV technique. The CV was recorded repeatedly with the Fe−Cu−rGO@Ag sensor for 10 cycles at a 50 mV/s scan rate. The CV graph shows no significant change in both the peak potential and current density of creatinine oxidation for 10 cycles, as shown in Figure S7a. The scatter chart shows the current density at each cycle, which remains almost constant with a relative standard deviation (RSD) of only 2.7% (Figure S7b).

To study the reproducibility of the Fe−Cu−rGO@Ag, four different sensors named Sensor-1,2,3,4 were obtained by electrodeposition and tested by CV techniques. Each modified electrode was scanned for 10 consecutive cycles at a scan rate of 50 mV/s within the range of −0.8 V + 0.8 V to −0.8 V potential in 0.01 M PBS containing 100 μM creatinine. The scanning results of the last cycle are shown in Figure S8a. The relative standard deviation of the oxidation peak current density is only 2.0% (Figure S8b), indicating that Fe−Cu−rGO@Ag has a good reproducibility in sensing applications. For the sensor stability and reusability study, a single sensor is used for creatinine detections periodically for 10 weeks. After each week, the CV scan is performed for 10 consecutive cycles in 0.01 M PBS containing 100 μM creatinine at a scan rate of 50 mV/s. It is found that the stability of the electrode is not lost even after 6 weeks, as shown in Figure S9.[59] The oxidation peak current density remains more than 90% of the initial value up to 6 weeks; however, the oxidation peak current density gradually decreases from the seventh week (66%), signifying that the nanocomposite has good stability for up to 6 weeks. The overall study demonstrates that the present electrochemical sensor, Fe−Cu−rGO@Ag, can provide good repeatability, reproducibility, and stability for creatinine detection even after repeated use, which is a fundamental requirement for an electrochemical-based sensor development under point-of-care settings. It is to note that, after every use, the sensor electrode was washed in PBS (0.01 M) and stored at ambient temperature.[49]

Sensor Selectivity. To evaluate any sensor's commercial importance, it is essential to investigate the selectivity of the same toward various possible interfering molecules. Fe−Cu−rGO@Ag was tested toward uric acid, urea, dopamine, and glutathione, which potentially coexist with creatinine in the blood to determine the interfering effects. Uric acid, urea, dopamine, and glutathione were tested at their detectable concentrations, i.e., uric acid, 100.0 μM; urea, 1.0 mM; dopamine, 100.0 μM; and glutathione, 50.0 μM in 0.01 M PBS (pH 7.4) in the presence of 100 μM creatinine. The modified electrode is sensitive and selective even in the presence of such commonly interfering species.[16] In Figure S10, -b, the prominent CV and DPV peaks for dopamine, urea, creatinine, glutathione, and uric acid are observed. The potential difference of 40 and 90 mV between dopamine and urea for CV and DPV are recorded, respectively. Whereas 80 mV (CV) and 210 mV (DPV) potential differences are recorded between urea and creatinine. Similarly, creatinine and glutathione are 250 mV (CV) and 210 mV (DPV) apart. In comparison, the difference between glutathione and uric acid is approximately 210 mV (CV) and 240 mV (DPV), as shown in Figure S10a, b. This result indicates that the present sensor, Fe−Cu−rGO@Ag, is specific to creatinine and does not interfere with

https://doi.org/10.1021/acsbiomaterials.1c00484
ACS Biomater. Sci. Eng. XXXX, XXX, XXX−XXX

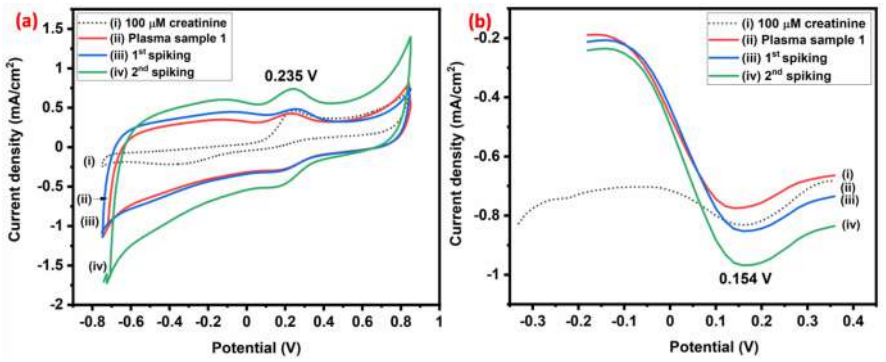

Figure 7. (a) CV at a scan rate of 50 mV/s and (b) DPV using the Fe−Cu−rGO@Ag electrode with 100 μM creatinine (i; dotted line), blood plasma sample 1 (ii; red line), blood plasma spiked with 100 μM creatinine (iii; blue line) and blood plasma spiked with 250 μM creatinine (iv; green line).

commonly available plasma bioanalytes like uric acid, urea, dopamine, and glutathione.

Analysis with Whole Blood. The analytical performance of the Fe−Cu−rGO@Ag electrochemical sensor was checked by determining the presence of creatinine in whole blood samples. Three blood samples were collected from DSP Hospital with the consent of healthy volunteers. The blood samples were used as received without any further treatment. A plasma separation membrane was used to separate the plasma from the whole blood to the detection zone, as shown in Figure S11. The CV and DPV graphs were recorded to see the creatinine concentration, which was initially present in the blood. CV and DPV values of 0.425 and −0.77 mA/cm^2 current density are recorded respectively for sample 1, as shown in Figure 7a, b. The already present creatinine concentration is determined by correlating the observed current density values with the linear graph obtained from the concentration study during sensitivity measurements. The result shows ∼90 μM of creatinine in the collected blood sample.

To check the repeatability of the result, we performed the experiment three times, and current density values of 0.42, 0.426, and 0.431 mA/cm^2 were observed for sample 1. Plasma samples were then spiked with 100 and 250 μM creatinine, and it is found that on adding more creatinine to the blood, a noticeable change in anodic peak occurs from the baseline. The study shows that the clinically determined concentration (by following standard testing protocol at DSP Hospital) is almost equal to the estimated creatinine concentration after spiking with 250 μM (2nd spiking) of creatinine. The change in current density at the peak voltage (Figure 7a-iii,iv) is 0.249 mA/cm^2, which signifies the fact that the current density changes by 1.0 μA μM^{-1} cm^{-2} with an average recovery of 97.84% (sample 1; Table S5). Similarly, the average recovery of 98.01 and 100.07% is obtained for samples 2 and 3, respectively (Table S5 and Figure S12). It could be observed that on spiking of 250 μM (2nd spiking) of creatinine, the change in current density at the peak voltage is 0.287 mA/cm^2 (sample 2, Figure S12aii-iii) and 0.282 mA/cm^2 (sample 3, Figure S12bii-iii) inferring the fact that current density changes by 1.14 and 1.12 μA μM^{-1} cm^{-2} of creatinine for samples 2 and 3 respectively. In Figure 5c, the sensitivity test with creatinine solution is found to be 1.1 μA μM^{-1} cm^{-2}. As the calculated sensitivity during experiments with whole blood samples closely matches the tested sensitivity for creatinine solution obtained from the concentrations versus the current density curve (Figure 5c), it is confirmed that the chip shows consistent sensitivity in the presence of real blood samples. Furthermore, the absence of any additional peaks near 0.235 V (peak voltage for creatinine) establishes that the chip has high sensitivity and is selective toward creatinine detection, even in whole blood samples.

Reusability of the Electrochemical Sensing Chip (Proposed POC). It is also worth exploring the reusability of the sensor, Fe−Cu−rGO@Ag, in the blood sample. As blood plasma was absorbed on the plasma separation membrane's surface placed over the electrodes during plasma creatinine detection, it could not be reused. However, the sensor, Fe−Cu−rGO@Ag, may be used after cleaning with PBS. To check this aspect, we washed the counter electrode and the working electrode Fe−Cu−rGO@Ag, which were present in the electrochemical sensing chip, with 0.01 M PBS after performing experiments with blood sample 1 (Figure 7), and CV was carried out with PBS for 50 cycles at a 50 mV/s scan rate from −1 V to +1 V and back to −1 V. The graph of Figure S13 shows no redox peak in the CV in the presence of PBS. The result indicates that the cleaning procedure successfully refreshed the electrode surface for another use.[60] Additionally, this washed sensor was used to perform experiments with blood samples 2 and 3, and peaks for creatinine could be detected precisely (Figure S12a, b), confirming the reusability and stability of the sensor.

CONCLUSION

In conclusion, we developed a nonenzymatic sensor for creatinine detection in an electrochemical sensing chip. Reduced graphene oxide stabilized binary iron−copper nanocomposite over 3-D printed Ag electrode (Fe−Cu−rGO@Ag), serving as a sensor, was prepared stepwise; electrodeposition of reduced graphene oxide (rGO) followed by binary iron−copper nanoparticles on rGO@3D printed Ag electrode. The FESEM, EDS, XPS, XRD, and Raman studies confirmed the presence of iron and copper nanoparticles in Fe_2O_3 and Cu^0 states with a size range of ∼15−16 nm, which made the overall sensor system electrocatalytically efficient for rapid and sensitive detection of creatinine. The sensing performance of Fe−Cu−rGO@Ag was demonstrated through cyclic voltammetry, differential pulse voltammetry, and electrochemical impedance spectroscopy techniques. The current density in mA/cm^2 range against the creatinine concentrations showed the excellent catalytic response in the range of 0.01 μM to 1000 μM with the limit of detection of

https://doi.org/10.1021/acsbiomaterials.1c00484
ACS Biomater. Sci. Eng. XXXX, XXX, XXX−XXX

0.01 μM (10 nM) and a sensitivity of 1.1 μA μM^{-1} cm^{-2} at the physiological pH, making it highly suitable for accurate blood creatinine analysis. The mechanism involves the synergistic effect of copper−iron oxide binary nanoparticles, where Fe atoms of Fe_2O_3 act as active sites for creatinine oxidation through the secondary amine nitrogen, and the CuNP acts as an excellent electron-transfer mediator through rGO. The repeatability, reproducibility, stability, and reusability of the sensor were evaluated to demonstrate its potential to be used as creatinine sensing applications. The sensor was highly sensitive and selective toward creatinine even in the presence of uric acid, glutathione, dopamine and urea as commonly interfering species. The detection method was successfully applied to determine the creatinine level in the blood plasma after separating from whole blood using a plasma separation membrane in the same electrochemical sensing chip. The observed results are comparable or better than the reported detection techniques and conventional clinical methods for blood creatinine, reiterating the benefit of the developed sensor for POC application.

■ ASSOCIATED CONTENT

Supporting Information

The Supporting Information is available free of charge at https://pubs.acs.org/doi/10.1021/acsbiomaterials.1c00484.

Electrochemical detection of creatinine by various research groups (Table S1); Randles equivalent circuit values recorded with different electrodes (Table S2); calculated values of coefficients (Table S3); calculated values of α, D, C, and K^0 for $Fe(CN)_6^{3-/4-}$ and creatinine (Table S4); creatinine spiking in blood plasma samples (Table S5); electrodeposition of rGO, Fe, Cu (Figure S1); Raman spectra of Fe−Cu−rGO and GO (Figure S2); electrochemical investigation of Cu^0 and Fe^{3+} using 0.1 M NaOH (Figure S3); 3D printed Ag electrodes and dimensions (Figure S4); electrochemical performance analysis of sensor with creatinine (Figure S5); oxime formation on the PSM (Figure S6); repeatability study (Figure S7); reproducibility study (Figure S8); stability study (Figure S9); selectivity study (Figure S10); plasma separation on chip (Figure S11); spiking study in blood sample (Figure S12); reusability study of the sensor (Figure S13) (PDF)

■ AUTHOR INFORMATION

Corresponding Authors

Nripen Chanda − *Materials Processing and Microsystems Laboratory, CSIR-Central Mechanical Engineering Research Institute, Durgapur, West Bengal 713209, India; Academy of Scientific and Innovative Research (AcSIR), Ghaziabad, Uttar Pradesh 201002, India;* orcid.org/0000-0002-9902-5595; Phone: +91-9933034370; Email: n_chanda@cmeri.res.in

Soumen Mandal − *Materials Processing and Microsystems Laboratory, CSIR-Central Mechanical Engineering Research Institute, Durgapur, West Bengal 713209, India; Academy of Scientific and Innovative Research (AcSIR), Ghaziabad, Uttar Pradesh 201002, India;* orcid.org/0000-0002-7353-0067; Phone: +91-9476326532; Email: somandal88@cmeri.res.in

Authors

Preeti Singh − *Materials Processing and Microsystems Laboratory, CSIR-Central Mechanical Engineering Research Institute, Durgapur, West Bengal 713209, India; Academy of Scientific and Innovative Research (AcSIR), Ghaziabad, Uttar Pradesh 201002, India*

Debolina Roy − *Materials Processing and Microsystems Laboratory, CSIR-Central Mechanical Engineering Research Institute, Durgapur, West Bengal 713209, India; Academy of Scientific and Innovative Research (AcSIR), Ghaziabad, Uttar Pradesh 201002, India*

Complete contact information is available at: https://pubs.acs.org/10.1021/acsbiomaterials.1c00484

Funding

This research was financially supported by the Department of Science and Technology-SERB, India (Award EMR/2017/002948).

Notes

The authors declare no competing financial interest.

■ ACKNOWLEDGMENTS

The authors gratefully acknowledge Dr. Harish Hirani, Director of CMERI, Durgapur, and Dr. Nilrudra Mandal, Head, Material Processing and Microsystems Laboratory, CMERI, Durgapur, for their encouragement and support. Durgapur Steel Plant (DSP) Hospital, West Bengal, India, is gratefully acknowledged for providing blood samples to carry out experiments.

■ REFERENCES

(1) Chapter 1: Definition and Classification of CKD. *Kidney Int. Suppl.* **2013**, *3* (1), 19−62.

(2) Lad, U.; Khokhar, S.; Kale, G. M. Electrochemical Creatinine Biosensors. *Anal. Chem.* **2008**, *80* (21), 7910−7917.

(3) Wang, L.; Chen, M.; He, R.; Sun, Y.; Yang, J.; Xiao, L.; Cao, J.; Zhang, H.; Zhang, C. Serum Creatinine Distinguishes Duchenne Muscular Dystrophy from Becker Muscular Dystrophy in Patients Aged ≤ 3 Years: A Retrospective Study. *Front. Neurol.* **2017**, *8*, DOI: 10.3389/fneur.2017.00196.

(4) Mahmood, R. T.; Asad, M. J.; Noorulamin, M.; Ul Amin, N.; Mahmood, T.; Asad, M. J.; Zafar, M.; Mehmood Raja, A. Evaluating Urea and Creatinine Levels in Chronic Renal Failure Pre and Post Dialysis: A Prospective Study Expression and Mutational Analysis of Genes Involved in Vitamin D Converting Enzymes View Project Evaluating Urea and Creatinine Levels in Chronic Re. *J. Cardiovasc. Dis.* **2014**, *2* (2), 2330−2460.

(5) Theadom, A.; Rodrigues, M.; Roxburgh, R.; Balalla, S.; Higgins, C.; Bhattacharjee, R.; Jones, K.; Krishnamurthi, R.; Feigin, V. Prevalence of Muscular Dystrophies: A Systematic Literature Review. *Neuroepidemiology* **2014**, *43* (3−4), 259−268.

(6) Bikbov, B.; Purcell, C. A.; Levey, A. S.; Smith, M.; Abdoli, A.; Abebe, M.; Adebayo, O. M.; Afarideh, M.; Agarwal, S. K.; Agudelo-Botero, M.; et al. Global, Regional, and National Burden of Chronic Kidney Disease, 1990−2017: A Systematic Analysis for the Global Burden of Disease Study 2017. *Lancet* **2020**, *395* (10225), 709−733.

(7) Du, H.; Chen, R.; Du, J.; Fan, J.; Peng, X. Gold Nanoparticle-Based Colorimetric Recognition of Creatinine with Good Selectivity and Sensitivity. *Ind. Eng. Chem. Res.* **2016**, *55* (48), 12334−12340.

(8) Erenas, M. M.; Ortiz-Gómez, I.; De Orbe-Payá, I.; Hernández-Alonso, D.; Ballester, P.; Blondeau, P.; Andrade, F. J.; Salinas-Castillo, A.; Capitán-Vallvey, L. F. Ionophore-Based Optical Sensor for Urine Creatinine Determination. *ACS Sensors* **2019**, *4* (2), 421−426.

(9) Sierra, A. F.; Hernández-Alonso, D.; Romero, M. A.; González-Delgado, J. A.; Pischel, U.; Ballester, P. Optical Supramolecular Sensing of Creatinine. *J. Am. Chem. Soc.* **2020**, *142* (9), 4276−4284.
(10) Mora, L.; Sentandreu, M. A.; Toldrá, F. Hydrophilic Chromatographic Determination of Carnosine, Anserine, Balenine, Creatine, and Creatinine. *J. Agric. Food Chem.* **2007**, *55* (12), 4664−4669.
(11) Randviir, E. P.; Banks, C. E. Analytical Methods for Quantifying Creatinine within Biological Media. *Sens. Actuators, B* **2013**, *183*, 239−252.
(12) Dasgupta, P.; Kumar, V.; Krishnaswamy, P. R.; Bhat, N. Biochemical Assay for Serum Creatinine Detection through a 1-Methylhydantoin and Cobalt Complex. *RSC Adv.* **2020**, *10* (64), 39092−39101.
(13) Kumar, P.; Jaiwal, R.; Pundir, C. S. An Improved Amperometric Creatinine Biosensor Based on Nanoparticles of Creatininase, Creatinase and Sarcosine Oxidase. *Anal. Biochem.* **2017**, *537*, 41−49.
(14) Cincotto, F. H.; Fava, E. L.; Moraes, F. C.; Fatibello-Filho, O.; Faria, R. C. A New Disposable Microfluidic Electrochemical Paper-Based Device for the Simultaneous Determination of Clinical Biomarkers. *Talanta* **2019**, *195*, 62−68.
(15) Kalasin, S.; Sangnuang, P.; Khownarumit, P.; Tang, I. M.; Surareungchai, W. Evidence of Cu (I) Coupling with Creatinine Using Cuprous Nanoparticles Encapsulated with Polyacrylic Acid Gel-Cu (II) in Facilitating the Determination of Advanced Kidney Dysfunctions. *ACS Biomater. Sci. Eng.* **2020**, *6* (2), 1247−1258.
(16) Raveendran, J.; Resmi, P. E.; Ramachandran, T.; Nair, B. G.; Satheesh Babu, T. G. Fabrication of a Disposable Non-Enzymatic Electrochemical Creatinine Sensor. *Sens. Actuators, B* **2017**, *243*, 589−595.
(17) Wen, T.; Zhu, W.; Xue, C.; Wu, J.; Han, Q.; Wang, X.; Zhou, X.; Jiang, H. Novel Electrochemical Sensing Platform Based on Magnetic Field-Induced Self-Assembly of Fe3O4@Polyaniline Nanoparticles for Clinical Detection of Creatinine. *Biosens. Bioelectron.* **2014**, *56*, 180−185.
(18) Randviir, E. P.; Kampouris, D. K.; Banks, C. E. An Improved Electrochemical Creatinine Detection Method via a Jaffe-Based Procedure. *Analyst* **2013**, *138* (21), 6565−6572.
(19) Sriramprabha, R.; Sekar, M.; Revathi, R.; Viswanathan, C.; Wilson, J. Fe2O3/Polyaniline Supramolecular Nanocomposite: A Receptor Free Sensor Platform for the Quantitative Determination of Serum Creatinine. *Anal. Chim. Acta* **2020**, *1137*, 103−114.
(20) Kalasin, S.; Sangnuang, P.; Khownarumit, P.; Tang, I. M.; Surareungchai, W. Salivary Creatinine Detection Using a Cu(I)/Cu(II) Catalyst Layer of a Supercapacitive Hybrid Sensor: A Wireless IoT Device to Monitor Kidney Diseases for Remote Medical Mobility. *ACS Biomater. Sci. Eng.* **2020**, *6* (10), 5895−5910.
(21) Wei, F.; Cheng, S.; Korin, Y.; Reed, E. F.; Gjertson, D.; Ho, C. M.; Gritsch, H. A.; Veale, J. Serum Creatinine Detection by a Conducting-Polymer-Based Electrochemical Sensor to Identify Allograft Dysfunction. *Anal. Chem.* **2012**, *84* (18), 7933−7937.
(22) Diouf, A.; Motia, S.; El Alami El Hassani, N.; El Bari, N.; Bouchikhi, B. Development and Characterization of an Electrochemical Biosensor for Creatinine Detection in Human Urine Based on Functional Molecularly Imprinted Polymer. *J. Electroanal. Chem.* **2017**, *788*, 44−53.
(23) Dasgupta, P.; Kumar, V.; Krishnaswamy, P. R.; Bhat, N. Serum Creatinine Electrochemical Biosensor on Printed Electrodes Using Monoenzymatic Pathway to 1-methylhydantoin Detection. *ACS Omega* **2020**, *5* (35), 22459−22464.
(24) Gao, X.; Gui, R.; Guo, H.; Wang, Z.; Liu, Q. Creatinine-Induced Specific Signal Responses and Enzymeless Ratiometric Electrochemical Detection Based on Copper Nanoparticles Electrodeposited on Reduced Graphene Oxide-Based Hybrids. *Sens. Actuators, B* **2019**, *285*, 201−208.
(25) Kalaivani, G. J.; Suja, S. K. Enzyme-Less Sensing of the Kidney Dysfunction Biomarker Creatinine Using an Inulin Based Bio-Nanocomposite. *New J. Chem.* **2019**, *43* (15), 5914−5924.
(26) Pandey, I.; Bairagi, P. K.; Verma, N. Electrochemically Grown Polymethylene Blue Nanofilm on Copper-Carbon Nanofiber Nanocomposite: An Electrochemical Sensor for Creatinine. *Sens. Actuators, B* **2018**, *277* (March), 562−570.
(27) Ponnaiah, S. K.; Prakash, P. Carbon Dots Doped Tungstic Anhydride on Graphene Oxide Nanopanels: A New Picomolar-Range Creatinine Selective Enzymeless Electrochemical Sensor. *Mater. Sci. Eng., C* **2020**, *113* (April), 111010.
(28) Fava, E. L.; Prado, T. M.; Garcia-Filho, A.; Silva, T. A.; Cincotto, F. H.; Cruz de Moraes, F.; Faria, R. C.; Fatibello-Filho, O. Non-Enzymatic Electrochemical Determination of Creatinine Using a Novel Screen-Printed Microcell. *Talanta* **2020**, *207*, 120277.
(29) Park, J.; Dattatraya Saratale, G.; Cho, S. K.; Bae, S. Synergistic Effect of Cu Loading on Fe Sites of Fly Ash for Enhanced Catalytic Reduction of Nitrophenol. *Sci. Total Environ.* **2020**, *705*, 134544.
(30) Gupta, V. K.; Atar, N.; Yola, M. L.; Üstündağ, Z.; Uzun, L. A Novel Magnetic Fe@Au Core-Shell Nanoparticles Anchored Graphene Oxide Recyclable Nanocatalyst for the Reduction of Nitrophenol Compounds. *Water Res.* **2014**, *48* (1), 210−217.
(31) Jin, H.; Guo, H.; Gao, X.; Gui, R. Selective and Sensitive Electrochemical Sensing of Gastrodin Based on Nickel Foam Modified with Reduced Graphene Oxide/Silver Nanoparticles Complex-Encapsulated Molecularly Imprinted Polymers. *Sens. Actuators, B* **2018**, *277*, 14−21.
(32) Jin, H.; Zhao, C.; Gui, R.; Gao, X.; Wang, Z. Reduced Graphene Oxide/Nile Blue/Gold Nanoparticles Complex-Modified Glassy Carbon Electrode Used as a Sensitive and Label-Free Aptasensor for Ratiometric Electrochemical Sensing of Dopamine. *Anal. Chim. Acta* **2018**, *1025*, 154−162.
(33) Priyadarsini, S.; Mohanty, S.; Mukherjee, S.; Basu, S.; Mishra, M. Graphene and Graphene Oxide as Nanomaterials for Medicine and Biology Application. *J. Nanostructure Chem.* **2018**, *8* (2), 123−137.
(34) Browne, M. P.; Novotný, F.; Sofer, Z.; Pumera, M. 3D Printed Graphene Electrodes' Electrochemical Activation. *ACS Appl. Mater. Interfaces* **2018**, *10* (46), 40294−40301.
(35) Foo, C. Y.; Lim, H. N.; Mahdi, M. A.; Wahid, M. H.; Huang, N. M. Three-Dimensional Printed Electrode and Its Novel Applications in Electronic Devices. *Sci. Rep.* **2018**, *8* (1), 1−11.
(36) Li, W.; Yang, S.; Shamim, A. Screen Printing of Silver Nanowires: Balancing Conductivity with Transparency While Maintaining Flexibility and Stretchability. *npj Flex. Electron.* **2019**, *3* (1), 13.
(37) Fernandes, I. J.; Aroche, A. F.; Schuck, A.; Lamberty, P.; Peter, C. R.; Hasenkamp, W.; Rocha, T. L. A. C. Silver Nanoparticle Conductive Inks: Synthesis, Characterization, and Fabrication of Inkjet-Printed Flexible Electrodes. *Sci. Rep.* **2020**, *10* (1), 1−11.
(38) Marcano, D. C.; Kosynkin, D. V.; Berlin, J. M.; Sinitskii, A.; Sun, Z.; Slesarev, A.; Alemany, L. B.; Lu, W.; Tour, J. M. Improved Synthesis of Graphene Oxide. *ACS Nano* **2010**, *4* (8), 4806−4814.
(39) Alonso, R. M.; San-Martín, M. I.; Sotres, A.; Escapa, A. Graphene Oxide Electrodeposited Electrode Enhances Start-up and Selective Enrichment of Exoelectrogens in Bioelectrochemical Systems. *Sci. Rep.* **2017**, *7* (1), 1−10.
(40) Luo, B.; Li, X.; Yang, J.; Li, X.; Xue, L.; Li, X.; Gu, J.; Wang, M.; Jiang, L. Non-Enzymatic Electrochemical Sensors for the Detection of Hydrogen Peroxide Based on Cu2O/Cu Nanocomposites. *Anal. Methods* **2014**, *6* (4), 1114−1120.
(41) Paulraj, A. R.; Kiros, Y.; Skårman, B.; Vidarsson, H. Core/Shell Structure Nano-Iron/Iron Carbide Electrodes for Rechargeable Alkaline Iron Batteries. *J. Electrochem. Soc.* **2017**, *164* (7), A1665−A1672.
(42) Chatterjee, B. K.; Bhattacharjee, K.; Dey, A.; Ghosh, C. K.; Chattopadhyay, K. K. Influence of Spherical Assembly of Copper Ferrite Nanoparticles on Magnetic Properties: Orientation of Magnetic Easy Axis. *Dalt. Trans.* **2014**, *43* (21), 7930−7944.
(43) Dubale, A. A.; Su, W. N.; Tamirat, A. G.; Pan, C. J.; Aragaw, B. A.; Chen, H. M.; Chen, C. H.; Hwang, B. J. The Synergetic Effect of Graphene on Cu2O Nanowire Arrays as a Highly Efficient Hydrogen

https://doi.org/10.1021/acsbiomaterials.1c00484
ACS Biomater. Sci. Eng. XXXX, XXX, XXX−XXX

Evolution Photocathode in Water Splitting. *J. Mater. Chem. A* **2014**, *2* (43), 18383−18397.
(44) Dan, H.; Kong, Y.; Yue, Q.; Liu, J.; Xu, X.; Kong, W.; Gao, Y.; Gao, B. Magnetic Field-Enhanced Radical Intensity for Accelerating Norfloxacin Degradation under FeCu/RGO Photo-Fenton Catalysis. *Chem. Eng. J.* **2020**, 127634.
(45) Singh, P.; Nath, P.; Arun, R. K.; Mandal, S.; Chanda, N. Novel Synthesis of a Mixed Cu/CuO-Reduced Graphene Oxide Nanocomposite with Enhanced Peroxidase-like Catalytic Activity for Easy Detection of Glutathione in Solution and Using a Paper Strip. *RSC Adv.* **2016**, *6* (95), 92729−92738.
(46) Xia, Y.; He, Z.; Su, J.; Tang, B.; Liu, Y. Enhanced Photocatalytic Performance of Z-Scheme Cu2O/Bi5O7I Nanocomposites. *J. Mater. Sci.: Mater. Electron.* **2018**, *29* (17), 15271−15281.
(47) Konwar, A.; Kalita, S.; Kotoky, J.; Chowdhury, D. Chitosan-Iron Oxide Coated Graphene Oxide Nanocomposite Hydrogel: A Robust and Soft Antimicrobial Biofilm. *ACS Appl. Mater. Interfaces* **2016**, *8* (32), 20625−20634.
(48) Ige, E. O.; Arun, R. K.; Singh, P.; Gope, M.; Saha, R.; Chanda, N.; Chakraborty, S. Water Desalination Using Graphene Oxide-Embedded Paper Microfluidics. *Microfluid. Nanofluid.* **2019**, *23* (6), 1−8.
(49) Singh, P.; Chatterjee, M.; Chatterjee, K.; Arun, R. K.; Chanda, N. Design of a Point-of-Care Device for Electrochemical Detection of P.Vivax Infected-Malaria Using Antibody Functionalized RGO-Gold Nanocomposite. *Sens. Actuators, B* **2021**, *327*, 128860.
(50) Li, S. J.; Xing, Y.; Hou, L. L.; Feng, Z. Q.; Tian, Y.; Du, J. M. Facile Synthesis of NiO/CuO/Reduced Graphene Oxide Nanocomposites for Use in Enzyme-Free Glucose Sensing. *Int. J. Electrochem. Sci.* **2016**, *11* (8), 6747−6760.
(51) Müller-Zülow, B.; Kipp, S.; Lacmann, R.; Schneeweiss, M. A. Topological Aspects of Iron Corrosion in Alkaline Solution by Means of Scanning Force Microscopy (SFM). *Surf. Sci.* **1994**, *311* (1−2), 153−158.
(52) Park, H.; Hwang, S. J.; Kim, K. An Electrochemical Detection of Hg 2 + Ion Using Graphene Oxide as an Electrochemically Active Indicator. *Electrochem. Commun.* **2012**, *24* (1), 100−103.
(53) Bharti, A.; Agnihotri, N.; Prabhakar, N. A Voltammetric Hybridization Assay for MicroRNA-21 Using Carboxylated Graphene Oxide Decorated with Gold-Platinum Bimetallic Nanoparticles. *Microchim. Acta* **2019**, *186* (3), 185.
(54) Bojang, A. A.; Wu, H. S. Characterization of Electrode Performance. *Catalysts* **2020**, *10* (Cv), 782.
(55) Wang, H.; Sayed, S. Y.; Luber, E. J.; Olsen, B. C.; Shirurkar, S. M.; Venkatakrishnan, S.; Tefashe, U. M.; Farquhar, A. K.; Smotkin, E. S.; McCreery, R. L.; Buriak, J. M. Redox Flow Batteries: How to Determine Electrochemical Kinetic Parameters. *ACS Nano* **2020**, *14* (3), 2575−2584.
(56) Sharma, A.; Rawat, K.; Bohidar, H. B.; Solanki, P. R. Studies on Clay-Gelatin Nanocomposite as Urea Sensor. *Appl. Clay Sci.* **2017**, *146* (June), 297−305.
(57) Brown, A. P.; Anson, F. C. Electron Transfer Kinetics with Both Reactant and Product Attached to the Electrode Surface. *J. Electroanal. Chem. Interfacial Electrochem.* **1978**, *92* (2), 133−145.
(58) Bhargava, S. P.; Sogani, N. C. A New Spot Test for Oximes. *Microchim. Acta* **1971**, *59* (2), 391−392.
(59) Aparna, T. K.; Sivasubramanian, R.; Dar, M. A. One-Pot Synthesis of Au-Cu2O/RGO Nanocomposite Based Electrochemical Sensor for Selective and Simultaneous Detection of Dopamine and Uric Acid. *J. Alloys Compd.* **2018**, *741*, 1130−1141.
(60) Chang, F.; Xie, X.; Li, M.; Zhu, Z. A Miniaturized Electrochemical Device Integrating a Biconical Microchannel and Carbon Fiber Disk Ultramicroelectrode. *Analyst* **2016**, *141* (16), 4859−4862.

https://doi.org/10.1021/acsbiomaterials.1c00484
ACS Biomater. Sci. Eng. XXXX, XXX, XXX−XXX